ASTRO2020 APC White Paper

HEX-P: The High-Energy X-ray Probe

<u>Thematic area</u>: Space Based Probe class Project, Formation and Evolution of Compact Objects, Cosmology and Fundamental Physics, Stars and Stellar Evolution, Resolved Stellar Populations and their Environments, Galaxy Evolution, Multi-Messenger Astronomy and Astrophysics.

Principal Author:
Name: Kristin K. Madsen
Institution: California Institute of Technology
Email: kkm@caltech.edu
Phone: 626 395 6634

Co-authors:

D. Alexander, Durham University
M. Bachetti, INAF-Osservatorio Astronomico di Cagliari
D. Ballantyne, Georgia Institute of Technology
M. Baloković, Center for Astrophysics | Harvard & Smithsonian
S. Boggs, USD
P. Boorman, University of Southampton
N. W. Brandt, Penn State
L. Brenneman, Center for Astrophysics | Harvard & Smithsonian
F. Christensen, DTU Space
F. Civano, Center for Astrophysics | Harvard & Smithsonian
R. Connors, Caltech
M. Descalle, LLNL
M. Elvis, Center for Astrophysics |

Harvard & Smithsonian
A. Fabian, University of Cambridge
D. Ferreira, DTU Space
F. Fornasini, , Center for Astrophysics | Harvard & Smithsonian
F. Fuerst, Quasar Ltd. for ESA
J. García, Caltech
N. Gellert, DTU Space
B. Grefenstette, Caltech
J. Grindlay, Harvard
M. Heida, Caltech
R. Hickox, Dartmouth
H. Miyasaka, Caltech
A. Hornschmeier, Goddard
A. Hornstrup, DTU Space
A. Jaodand, Caltech
N. Kamraj, Caltech
H. Krawczynski, Washington University

in St. Louis
G. Lansbury, Institute of Astronomy, Cambridge
A. Lohfink, Montana State University
G. Madejski, Standford
G. Matt, Roma Tre University
M. Middleton, University of Southampton
J. Miller, University of Michigan
S. Pike, Caltech
K. Pottschmidt, UMBC & NASA-GSFC
C. Ricci, Universidad Diego Portales
D. Stern, JPL/Caltech
J. Vogel, LLNL
D. Walton, University of Cambridge
J. Wilms, FAU Erlangen-Nuernberg
D. Wik, University of Utah
D. Windt, Reflective X-ray Optics LLC
W. Zhang, Goddard

Abstract:
The High-Energy X-ray Probe (HEX-P) is a next-generation high-energy X-ray observatory with broadband (2-200 keV) response that has 40 times the sensitivity of any previous mission in the 10-80 keV band and > 100 times the sensitivity of any previous mission in the 80-200 keV band. With this leap in observational capability, HEX-P will address a broad range of science objectives beyond any planned mission in the hard X-ray bandpass. HEX-P will probe the extreme environments around black holes and neutron stars, map the growth of supermassive black holes, and quantify the effect they have on their environments. HEX-P will resolve the hard X-ray emission from dense regions of our Galaxy to understand the high-energy source populations and investigate dark matter candidate particles through their decay channel signatures. If developed and launched on a timescale similar to Athena, the complementary abilities of the two missions will greatly enhance the Community's ability to address the important science questions of the hot universe. HEX-P addresses science that is not planned by any flagship-class missions, and is beyond the capability of an Explorer-class mission.

1. EXECUTIVE SUMMARY

The *Nuclear Spectroscopic Telescope Array* Small Explorer (*NuSTAR*; Harrison et al. 2013) opened the high-energy X-ray band, establishing the power of broad-band X-ray spectroscopy for probing the hot and energetic Universe. *NuSTAR* studies a diverse range of phenomena, from the regions near accreting black holes to the diffuse remnants of exploded stars. But as an Explorer, *NuSTAR* has limitations in sensitivity and angular resolution that leave a vast discovery space untouched. Furthermore, access to the high-energy band will likely disappear within a decade when *NuSTAR* de-orbits, closing this important window on the Universe. Any successor to *NuSTAR* should pursue a leap in performance to enable new science. However, such a leap is not possible in the current Explorer landscape.

The Probe class can make this possible. We describe the *High-Energy X-ray Probe* (*HEX-P*; Table 1), a Probe-class high-energy mission that will vastly extend the reach of broadband X-ray observations, with a factor of 40 improvement in sensitivity over *NuSTAR* in the 10-80 keV band, and a factor of ~100 improvement in sensitivity over current capabilities in the 80-200 keV band.

Synergies between observatories have been exemplified in this decade. With an early-2030s launch date, ESA's *Athena* mission will revolutionize high-resolution spectroscopy below 10 keV. With a well-matched launch, *HEX-P*'s high-energy (>10 keV) sensitivity will provide these two missions a powerful synergy for addressing a diverse range of questions central to modern astrophysics.

HEX-P utilizes advances in X-ray reflective coatings, optics, and detector technology made since *NuSTAR* was conceived. *HEX-P* has an angular resolution of 5″ (half-power diameter; HPD), an energy range of 2-

200 keV, and will operate primarily as a point-and-stare observatory with a funded, competitive Guest Observer (GO) program. The key *HEX-P* mission elements have strong *NuSTAR* heritage, and the instrument elements are based on existing technologies. The rough order-of-magnitude (ROM) cost is $800M (FY20), including launch and five years of operations.

2. SCIENCE GOALS AND OBJECTIVES

Broadband X-ray observations probe some of the most extreme regions in the universe, including shocks in supernovae explosions and merging galaxies, hot electron plasmas around black holes (BHs), and the strong magnetic fields of neutron stars (NSs). High-energy X-rays are also penetrating, enabling observations of objects veiled in large columns of dust and gas, from BHs embedded in dusty galaxies to compact objects hidden in the Milky Way. *HEX-P* brings together sensitivity from well below the iron line at 6-7 keV out to 10-40 keV, where the continuum in many sources changes rapidly and the hallmark reflection spectrum from dense material is evident, to several hundred keV, where extreme non-thermal processes dominate. Moreover, its high spatial resolution, low background, and precise timing performance allow for sensitive pulsation searches in crowded and distant fields where traditional high-sensitivity, low spatial resolution timing instruments fail. This makes *HEX-P* a unique astrophysical tool with a very broad reach. We describe here the primary objectives that drive the *HEX-P* design.

	NuSTAR	*Athena*/WFI	*HEX-P*
Bandpass	3-79 keV	0.2-15 keV	2-200 keV
Effective Area (@ 6 keV)	450 cm^2	2500 cm^2	4400 cm^2
Angular Resolution	60″	5″	5″
Spectral Resolution (FWHM)	600 eV @ 6 keV 1.2 keV @ 60 keV	170 eV @ 7 keV	200 eV @ 6 keV 0.8 keV @ 60 keV
Timing Resolution	1 μs	10 μs	1 μs
Field of View	13′× 13′	40′× 40′	13′× 13′

Table 1. *HEX-P performance parameters compared to NuSTAR and Athena.*
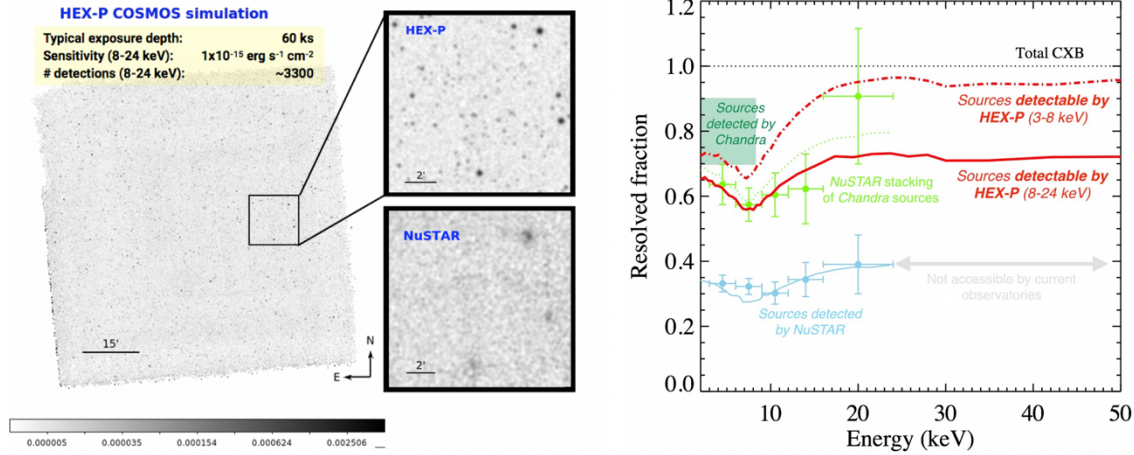
Figure 1. *Left: Simulation of a ~2 deg^2 HEX-P survey with an on-source exposure time of 60 ks. Right: Fraction of the CXB vs. energy resolved directly with NuSTAR (blue points) and Chandra (green box), and through NuSTAR stacking of Chandra sources (green points; Hickox et al., in prep.). Red lines show the model predictions for the resolved fraction for 8-24 keV HEX-P detections (sold line) and for stacking of 3-8 keV HEX-P detections (dot dashed line). Models are from Annana et al. (2019). HEX-P can directly resolve >70% of the 8-24 keV CXB and >90% through stacking.*

2.1. BLACK HOLE GROWTH OVER COSMIC TIME: A CENSUS OF OBSCURED AGN

For more details, see Astro2020 Science White Paper: "Resolving the Cosmic X-ray Background with a Next-generation High-energy X-ray Observatory" (Hickox, Civano, et al. 2019).

A complete census of Active Galactic Nuclei (AGN) activity is the foundation of any effort to understand the BH mass accretion history of the Universe, as well as the relationship between BH growth, environment, and host galaxy evolution. With a complete AGN census spanning a wide redshift and luminosity range, we can determine how BHs grow across cosmic time and reveal connections between BH accretion, their host galaxies, and large-scale structure.

The cosmic X-ray background (CXB), known to be produced primarily by AGN emission, peaks at energies of ~30 keV, implying a dominant population of AGN for which the lower-energy X-rays have been obscured by intervening gas. Many of these AGN are *extremely* obscured (i.e., Compton-thick, with an equivalent hydrogen column density $N_H > 10^{24}$ cm^{-2}; e.g., Gilli et al. 2007). Models suggest that these heavily obscured AGN may represent an early and rapid BH

growth phase (e.g., Hopkins et al. 2006, Blecha et al. 2018) that plays a critical role in the co-evolution of BHs and galaxies. To uncover this important "hidden" BH population, sensitive hard (i.e., high-energy; >10 keV) X-ray observations are essential.

Deep, soft (<10 keV) X-rays surveys with *Chandra* and *XMM-Newton* have provided the most sensitive low-energy probe of distant AGN activity to date (see Brandt & Alexander 2015 for a review). These surveys resolve <80% of the 0.6-6 keV CXB (Hickox & Markevitch 2006; Xue et al. 2012) and have informed synthesis models of the CXB, in which an evolving population of AGN is responsible for the integrated CXB spectrum (e.g., Ueda et al. 2014; Ananna et al. 2019).

However, a major challenge in interpreting CXB synthesis models has come from the limited observational constraints on the hard (>10 keV) X-ray emission for individual AGN. *NuSTAR* has carried out an extragalactic survey program covering well-studied fields with varying depth and area (e.g., COSMOS, ECDFS, EGS, UKIDSS UDS, HDFN). Together, these surveys have yielded ~300 hard X-ray selected AGN and have led to the most precise measurements to date above 10 keV of the X-ray number counts (log N-log S; Harrison et al. 2016), the X-ray luminosity function (Aird et al. 2015), and the evolution

of the obscuration distribution to z=3 (Del Moro et al. 2017, Zappacosta et al. 2018).

While revolutionary, *NuSTAR* still only probes the bright end of the hard X-ray population. The *NuSTAR* AGN sample is limited in both size and depth, probing above the knee of the luminosity function and missing the bulk of the population contributing to the total BH accretion density. Moreover, most sources are not detected in the hardest 8-24 keV band because of the rising background. *HEX-P* will provide the observational leap forward to uncover the complete population of obscured AGN. With 12 times better spatial resolution and an order-of-magnitude increase in effective area, *HEX-P* will, for the first time, probe the faint end of the hard X-ray luminosity function at z>0.5, providing a sample ~100 times larger than *NuSTAR*. Figure 1 (left) shows a simulated ~2 deg^2 COSMOS survey as seen with *HEX-P*: with the same 60 ks on-source exposure time as *NuSTAR*, *HEX-P* will reach a flux limit in the 8-24 keV band comparable to the flux limit reached by *Chandra* in the 2-10 keV band (with 160 ks on-source exposures). *HEX-P* will detect >3000 sources in this field alone. *HEX-P* surveys will measure the total BH accretion that produces the energy peak of the CXB, including *beyond* the CXB peak energy (>30 keV), where no detection has been found so far by *NuSTAR* (see Masini et al. 2018).

With a combination of surveys, *HEX-P* will directly resolve, for the first time, >70% of the CXB at its peak (compared to ~35% with *NuSTAR*; Harrison et al. 2016), a regime that so far has only been probed with stacking studies (Figure 1-right, solid red line). With its significantly improved PSF, hard X-ray stacking of 3-8 keV *HEX-P* detections will account for >90% of the CXB across a broad range of high energies (Figure 1-right, dot-dashed line). These *HEX-P* results will be crucial for CXB synthesis models (e.g., Annana et al. 2019).

In addition, *NuSTAR* has shown that many X-ray-detected AGN are significantly more obscured (up to Compton-thick columns) than can be determined through soft X-rays alone (e.g., Civano et al. 2015). Some luminous, obscured AGN lacking soft X-ray detections

remain extremely weak or undetected in deep *NuSTAR* exposures, implying $N_H \geq 10^{25}$ cm^{-2} (e.g., Stern et al. 2014, Yan et al. 2019). *NuSTAR* constraints indicate a large Compton-thick fraction, ~30% or higher (Lansbury et al. 2014, 2015). With its greatly enhanced sensitivity, *HEX-P* will revolutionize this science by finding and studying hundreds of very heavily obscured AGNs at energies above 8 keV, finally placing strong constraints on the Compton-thick fraction and its evolution with redshift and luminosity. Synergies with *JWST* will enable the study of the obscurer in the hard X-ray and mid-IR, providing the most complete view to date of the central engines in AGN across cosmic time.

2.2. PROBING THE POWER SOURCE IN ACCRETING BLACK HOLES AND COMPACT OBJECTS

For more details, see Astro2020 Science White Papers: "Probing the BH Engine with Relativistic X-ray Reflection Measurements" (García et al. 2019); "Probing the Physical Properties of the Corona in Accreting BHs" (Kamraj et al. 2019).

A detailed physical understanding of BH accretion remains lacking. Some of the accretion power is presumably supplied to an X-ray emitting corona though magnetic fields wound up by the disk. This heats coronal electrons, which then cool rapidly by Comptonizing the lower energy photons emitted by the accretion disc. The result is a hard X-ray power-law spectrum extending to just above the temperature of the bulk of the electrons. The coronal radiation illuminates the accretion disk, producing a reflection spectral component consisting of a forest of fluorescent lines, edges, and related features, with the most prominent being the Fe K emission complex near 6.4 keV. If originated near the BH, the spectral profiles are grossly distorted in the strong-gravity regime by Doppler effects, light bending, and gravitational redshift (Figure 2). Additionally, time delays between X-ray bands are typically observed due to differing light travel times for the direct and reflected radiation. Together, relativistic reflection and reverberation analysis enable us to map out the inner accretion flow as well as measure the spin of the BH.
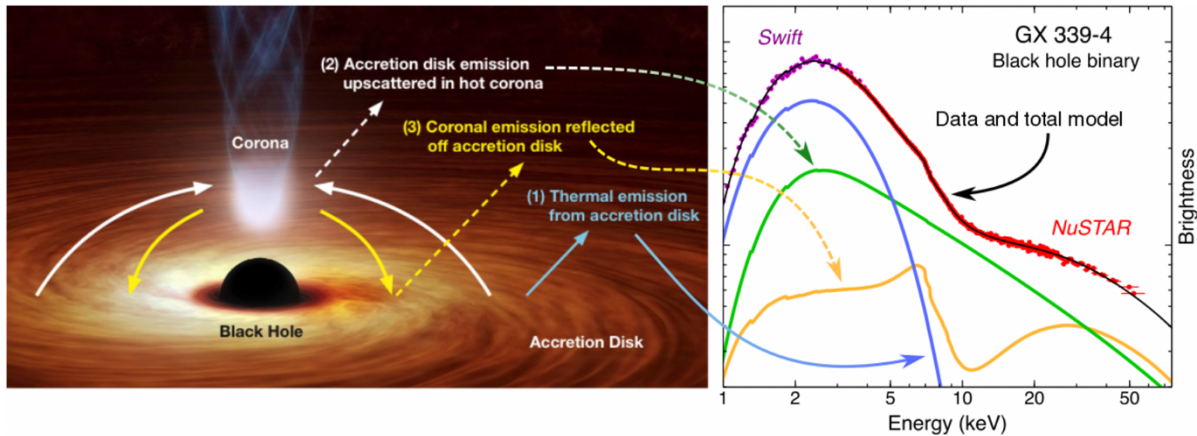
Figure 2. *The accretion disk radiates as a blackbody. In the inner regions, a compact corona (depicted here as the base of a jet) Compton up-scatters photons from the disk into a high-energy X-ray tail. This in turn irradiates the surface of the disk, producing a combination of back-scattered and fluorescent line emission, which peaks in the hard X-ray band (~20 keV). Broadband X-ray observations enable the robust determination of the relative contribution from each of these processes and probe the geometry of the innermost accretion flow.*

The geometry, location, and even the origin of the corona that illuminates the disk are still largely unknown. A number of studies agree on a compact region of Comptonizing hot electrons (e.g., Haardt 1993, Dove et al. 1997, Zdziarski et al. 2003), which may be associated with the base of a jet (e.g., Matt et al. 1992, Markoff et al. 2005). Recent *NuSTAR* observations show evidence for a thermal cutoff in the spectrum of several sources (e.g., Fabian et al. 2014, Lohfink et al. 2015, Lanzuisi et al. 2019), suggesting that the corona is close to the pair-thermostat limit (Fabian et al. 2015). Modeling the reflection spectrum accurately constrains the coronal electron temperature and optical depth, and indicates that the corona responds dramatically to changes in luminosity (García et al. 2015). This suggests a close connection between the corona and the accretion rate.

It is thus clear that understanding the physics of accretion necessitates understanding the connection between the corona and accretion disk. *HEX-P* will provide sensitive observations in the 2-200 keV band, an essential energy range for X-ray coronal reflection and reverberation studies. This requires good spectral resolution ($\leq$ 200 eV at 6 keV) and good timing capability ($\leq$10 μs). The spectral cut-off for most objects is predicted to occur at $\leq$ 200 keV. Of particular interest will be non-thermal tails and variations in apparent temperature with flux. Most targets will be variable, and it is important to have the sensitivity to follow the variability. *HEX-P* will also observe stellar mass Galactic BH binaries, some of which already show evidence for non-thermal tails in some flux states (e.g., Cyg X-1, GX 339-4). If their coronae are as compact as those of AGN, then the order of magnitude improvement in sensitivity provided by *HEX-P* will be required to follow the evolution of the corona on fast dynamical timescales. Amassing the evidence from all luminous accreting BHs will lead to ground-breaking advances in our understanding of coronae.

Accurate measurements of spins are crucial for understanding BH formation and evolution (e.g., Fragos & McClintock 2015), and for addressing the suggested correlation between jet power and BH spin (Narayan & McClintock 2012, Steiner et al. 2013, McClintock et al. 2014, Chen et al. 2016). HEX-P will provide data with the signal-to-noise and energy resolution to minimize (or completely remove) these model degeneracies. Simulations show that for a typical BH binary with a flux of 10 mCrab, a HEX-P exposure of 20 ks will simultaneously provide accurate estimates of both spin and inner radius. The excellent timing capabilities of HEX-P will allow further constraints on the models using reverberation studies in the time domain and

more advanced spectral-timing techniques (Uttley et al. 2014).

2.3. CONSTRAINING ENDPOINTS OF STELLAR EVOLUTION

For more details, see Astro2020 Science White Paper: "Breaking the Limit: Super-Eddington Accretion onto BHs and NSs" (Brightman et al. 2019).

Compact object demographics are key for constraining the final stages of stellar evolution (including supernova explosion models) and their dependence on metallicity. The hard X-ray band offers a window on the fate of the most massive stars – above 10 keV, the X-ray emission from normal galaxies is nearly completely dominated by NS and BH X-ray binary systems (e.g., Hornschemeier et al. 2016). Pulsations unambiguously identify NSs, and broadband observations extending above 10 keV can distinguish NSs from BHs based on luminosity and spectral hardness (Wik et al. 2014, Maccarone et al. 2016, Yukita et al. 2016, Lazzarini et al. 2018, Vulic et al. 2018).

The central regions of the Milky Way and nearby star-forming galaxies are key targets for such demographic studies. Theory predicts a large population of BH binaries in the central few parsecs of our Galaxy due to both dynamical settling and to the large population of massive stars resident there (Miralda-Escude & Gould 2000). Nearby star-forming galaxies are known to contain rich populations of binaries. However, while *NuSTAR* has made pioneering observations of the populations of

Science Goal	Observable	Requirement
G1. Resolve ≥70% of the CXB in the 8-30 keV band.	Number counts of hard X-ray sources in extragalactic field surveys.	• 10-30 keV sensitivity: ≤1×10^{-15} erg/s/cm^2 • PSF: ≤10″ (HPD)
G2. Measure distribution of supermassive BH spin in the local universe.	X-ray reflection spin estimates with ≤10% uncertainty for statistical sample of AGN.	• Band: 2-150 keV • Eff. Area: ≥10^3 cm^2 @ 6 keV • Resolution: ≤200 eV @ 6 keV
G3. Measure distribution of BH X-ray binary (BHXB) spins.	X-ray reflection spin estimates with ≤10% uncertainty for statistical sample of BHXBs.	• Band: 2-150 keV • Eff. Area: ≥10^3 cm^2 @ 6 keV • Resolution: ≤200 eV @ 6 keV • High count rate capabilities • Response time: ≤48 hr
G4. Investigate the origin, geometry, and behavior of the X-ray corona in accreting compact objects.	Coronal electron temperature and optical depth; emissivity of reflected emission; reverberation studies.	• Band: 2-200 keV • Eff. Area: ≥10^3 cm^2 @ 6 keV • Eff. Area: ≥10^2 cm^2 @ 200 keV • High count rate capabilities
G5. Understand the dynamics of BH accretion physics.	Level of disk truncation with ≤10% uncertainty and its outburst evolution for multiple BHXBs from X-ray reflection studies.	Met by G3 requirements.
G6. Find the hidden population of GC BHs and NSs.	Robust hardness and color of thousands of sources in the GC; pulsations from accreting NSs and magnetars close to Sgr A*.	• Band: 2-30 keV • Timing resolution: ≤10 μs • PSF: ≤10″ (HPD) • 10-30 keV sensitivity: ≤3×10^{-15} erg/s/cm^2
G7. Study the hard X-ray population of nearby galaxies.	Compact object type (BH vs. NS) for thousands of X-ray binaries from spectral and timing properties.	Met by G6 requirements.

Table 2. *Science requirements. Colors correspond to the three main science goals described in §2.*

binaries in the Galactic Center (GC) (Hong et al. 2016) and nearby star-forming galaxies (Hornschemeier et al. 2016), the arcminute angular resolution and limited sensitivity of *NuSTAR* have just scratched the surface of these studies.

In the GC, *HEX-P* will make dramatic advances in searching for postulated BH binaries and in identifying the fraction of the binary population with massive compact objects. BHs recently produced in the GC region will usually have main sequence O-star companions and be low-luminosity. *Chandra* discovered ~9,000 point sources in the central 2×0.8 deg^2 of the GC (Muno et al. 2009), of which *NuSTAR* only detected ~70 (Hong et al. 2016). *HEX-P* will detect the majority of these sources, including those in the central Galactic cusp. The broad *HEX-P* energy band will enable classification of the sources, distinguishing the unbroken power law tail of BH binaries from the optically thin thermal bremsstrahlung (with ionized Fe emission lines) of magnetic cataclysmic variables (CVs) and the hard spectra of pulsars. The improved angular resolution and high throughput of *HEX-P* will be essential for this work, which will yield important insights into the evolution of stellar populations over time in the GC.

NuSTAR found the GC pulsar (magnetar) J1745-2900 (Mori et al. 2014), and *HEX-P* will improve detection limits for GC pulsars by orders of magnitude with its sharper PSF and greater sensitivity. Pulsars can be powerful probes of the spacetime around Sgr A*. Pulsar timing can determine a star's orbital position to spectacular precision. Even relatively low-precision timing measurements (~0.1 ms) can measure the source position to within ~10 km, a precision orders of magnitude higher than achievable with radio or optical imaging. The detection of a pulsar population in the central parsec would measure the mass of Sgr A* with incredible precision (Psaltis et al. 2016). Such a pulsar population is predicted to exist, but has remained undetected thus far because of interstellar medium scattering and source confusion. Searches in the hard X-rays would be less affected by scattering, and would represent a complementary tool to high-frequency radio

searches planned from ngVLA or SKA-mid (e.g., Rajwade et al. 2017, Bower et al. 2018).

In nearby galaxies, *HEX-P* will identify thousands of BH and NS binaries, far beyond the modest sample of ~100 objects identified with *NuSTAR* to date. The broadband coverage will enable diagnostic diagrams that make use of spectral differences in binaries above 10 keV that are not apparent below 10 keV. Specifically, X-ray color-color plots using the 12-25 keV band show the first clear separation of NSs from BHs without making use of detailed timing information (e.g., Yukita et al. 2016). With its hard X-ray coverage, *HEX-P* will identify the accretion states of binaries, a key step towards understanding their accretion physics. With its additional improvement to pulsation searches, *HEX-P* will routinely look for pulsations in extragalactic X-ray binaries and ultraluminous X-ray sources (e.g., Bachetti et al. 2014, Fürst et al. 2016).

Theorists also predict a faint, non-thermal diffuse component to starburst galaxies that arises from Compton scattering of seed IR photons by charged particle populations (e.g., Wik et al. 2014). *HEX-P* will provide the first direct detection of this Inverse Compton emission, firmly establishing whether the leptonic models of particle acceleration are the correct prescription for the production of GeV gamma-ray emission in starburst galaxies.

3. TECHNICAL OVERVIEW

3.1. INSTRUMENT REQUIREMENTS

The instrument requirements for meeting the science goals are listed in Table 2. The high effective area requirement ($\geq 10^3$ cm^2 at 6 keV) is achieved by having three modules, and the required sensitivity through a combination of large effective area, low background, and compact PSF. A baseline PSF of 5″ (HPD) will be achieved through the use of monosilicate mirror technology, and the energy up to 200 keV reached by employing a 20 m long extendable mast, critical for obtaining the low gazing incidence angles, together with Ni/C+W/C multilayer coatings. Three pixelated CdTe detectors with heritage from *NuSTAR* provide detection capability for 2-200 keV.

Baseline Mission Parameters	
Orbit	LEO < 10° inclination
Altitude	600 km
Launch Vehicle	Falcon 9
Spacecraft	3-axis stabilized
Pointing Stability	2′
Pointing Accuracy	1′
Mission Life	5 yr
Power	900 W
Mass	1100 kg
Volume	2.2 m diam × 1.6 m height
Data Rate	2-60 GB/day

Table 3. *HEX-P baseline mission parameters.*

HEX-P will primarily operate as a point-and-stare observatory with a competitive, funded GO program. The spacecraft will have large sky accessibility to respond to Targets of Opportunity (ToOs), and the mission operations set up to handle fast ToOs.

3.2.   MISSION ARCHITECTURE

We baseline the mission design outlined in Table 3, with mass, power, and data-rate estimates scaled from *NuSTAR*. The spacecraft will be a 3-axis stabilized platform with a Sun-pointing solar array actuated on one-axis. We adopt a Low Earth Orbit (LEO), where reaction wheels with magnetic torque bars provide sub-arcminute pointing with no expendables. The spacecraft requirements are relatively unchallenging; the only technical issue is the 20 m mast, which, at the *HEX-P* mass, provides approximately 400 mN-meters of gravity gradient torque. This disturbance torque can be accommodated with standard reaction wheels but would require somewhat larger magnetic torque bars than is usual for this type of system; the mass of these bars is accounted for in the mission mass estimate.

4. TECHNOLOGY DRIVERS

The following sections briefly describe approaches to be studied for the optics and focal plane, which are the key instrument components.

4.1.   MULTILAYER HARD X-RAY OPTICS

NuSTAR utilizes Wolter-I conical approximation optics deposited with depth-graded W/Si and Pt/C multilayers to achieve its high-energy efficiency (Harrison et al. 2013). *HEX-P* will use Wolter-I optics with dimensions given in Table 4 (for details, see Madsen et al. 2018). Each *HEX-P* module is roughly the size of an *XMM-Newton* optic. There are two primary updates to the *NuSTAR* design for *HEX-P*: improving the angular resolution from 60″ to 5″ (HPD) and extending the energy band from 80 keV to 200 keV.

   Mirrors: *HEX-P* requires three identical mirror assemblies. They will be implemented using a technology being developed by the Next Generation X-ray Optics team at NASA's Goddard Space Flight Center (GSFC) (Zhang et al. 2019). The technology, having heritage in both *Chandra* and *NuSTAR*, is being developed for major missions such as *Lynx*, Probe missions such as *AXIS*, *TAP*, and *HEX-P*, as well as Explorer missions. The technology is based on polishing of mono-crystalline silicon and a modular integration approach. In the case of *HEX-P*, ~50,000 small mirror segments, each measuring 100 mm by 100 mm by 0.25 mm, will be fabricated, coated with multilayer coatings, integrated into 42 modules which will then be integrated into 9 meta-shells which, in turn, will be integrated into the three identical mirror assemblies. Each module weighs approximately 180 kg. The technical aspect unique to *HEX-P* is the mitigation of stress generated by the coatings. The thin film stress associated with the coatings, which distorts the figure of the mirror segments, is balanced by a layer of silicon oxide grown on the backside of each mirror segment, as illustrated in Figure 3. The basic validity of this process has been empirically demonstrated by Yao et al. (2019).

   Multilayers: Extending the bandpass from *NuSTAR*'s 80 keV to 200 keV involves avoiding the K-edges from Pt (78.4 keV) and
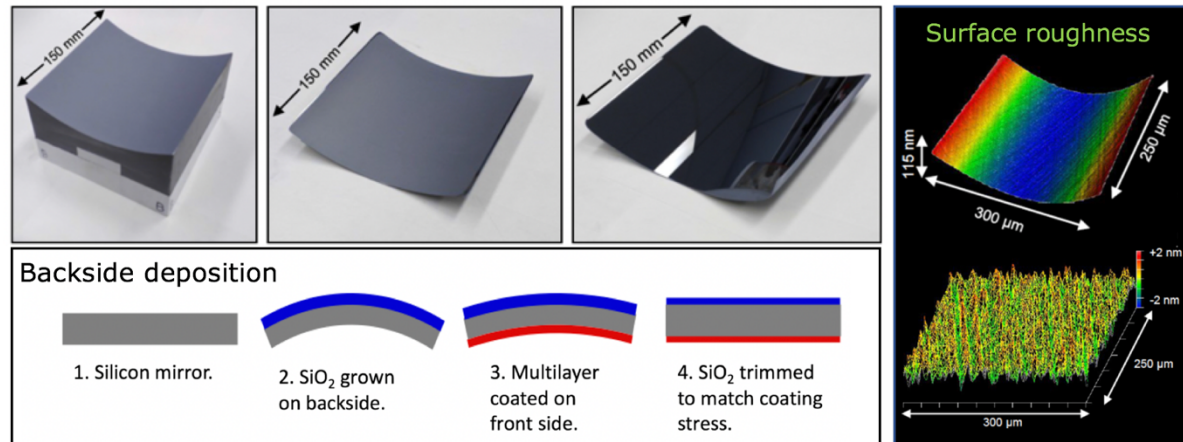
Figure 3. *Top: Segmented mirror production. Mirrors cut from a mono-crystalline silicon block are subsequently etched and polished into the desired shape. Bottom: Backside deposition to reduce stress. Right: Cylindrical interferometer measurements of a cylindrical mirror surface, showing full figure recovery.*

W (69.8 keV), which can be done by selecting material combinations that do not have strong edges in the primary band. Ni/C, which has been measured at 125 keV (Joensen et al. 1994), satisfies this demand and has demonstrated the low interface roughness and stability required for *HEX-P* (Girou et al. 2015). However, rather than a pure Ni/C multilayer stack, which tend to grow very thick for efficient reflection above 100 keV, *HEX-P* will employ a hybrid approach: the K-edges of Pt and W will be softened by combining a stack of Ni/C with already flight-proven coatings of W/C, W/Si, or WC/SiC. Ni/C will be used for the thicker layers. A hybrid coating design consisting of a W/C + Ni/C multilayer with a combined number of bi-layers similar to *NuSTAR*, has been shown to meet the effective area requirements for *HEX-P* (Gellert et al. 2019). The advantage to this method is thinner stacks, which reduces stress, and W/C, W/Si, and WC/SiC have low interface roughness (Wu et al. 2018), augmenting the off-axis response (Fernández-Perea et al. 2013, Brejnholt et al. 2014).

Some coating development work will be required to tune the Ni/C, W/C, and WC/SiC material combinations (W/Si is already well established from *NuSTAR*). However, the *NuSTAR* demonstrated versatility with three separate material combinations deposited with similar layer thickness and rates to the *HEX-P*

requirements provides confidence that the technological risk is low. Also, W-based coatings have been measured at energies above 100 keV with demonstrated performance that matches theoretical predictions at these energies (Windt et al. 2000, 2003, 2015). The overall Technological Readiness Level (TRL) of the multilayer coatings is therefore currently TRL 3 with active development studies underway to bring them to TRL 5 within a few years through development grants.

4.2.   FOCAL PLANE MODULES

The *HEX-P* focal plane is directly derived from technologies developed for *NuSTAR*. Each detector has a high-atomic number sensor (CdZnTe for *NuSTAR*, CdTe for *HEX-P*) coupled with a Caltech-designed custom readout funded by a current NASA APRA grant. This work is developing a next-generation application specific integrated unit (ASIC) using an improved fabrication process that reduces the component sizes while retaining the low-noise, low-power, high-performance characteristics of the *NuSTAR* ASIC. The pixel pitch will be reduced to 300 μm, as compared to the *NuSTAR* pixel pitch of 605 μm. Smaller pixels reduce the electronic noise, allowing for a lower trigger threshold and improved energy resolution at low energies.

	NuSTAR	*HEX-P*
Focal Length	10 m	20 m
# Shells	133	389
Min. Radius	54 mm	30 mm
Max. Radius	191 mm	350 mm
Shell Thickness	0.21 mm	0.25 mm
Multilayers	Pt/C, W/Si	Ni/C+W/C
Glass Mass / Optic	40 kg	180 kg

Table 4. HEX-P baseline optics parameters.

In addition to shrinking the pixel pitch, the *HEX-P* CdTe sensors will be 50% thicker than the *NuSTAR* CdZnTe sensors, which are 2 mm. This will increase the quantum efficiency at high energies, particularly above 70 keV, and achieve sensitivity up to 200 keV. The combination of smaller pixel pitch and thicker sensors will allow *HEX-P* to take greater advantage of the small pixel effect, a consequence of the Shockley-Ramo theorem of induced charge (Shockley 1938, Ramo 1939). In short, smaller pixels and thicker sensors lead to better detection of the motion of charge carriers in the sensor, resulting in improved energy resolution.

For a 20 m focal length and a field-of-view of 13′, the *HEX-P* detectors will need to provide an active region that spans at least 7.8 cm on a side, as compared to the *NuSTAR* active region, which is 4 cm on side. This requires a modest update to the focal plane form factor. Tiling this area with a 2×2 grid of arrays, as done with *NuSTAR*, requires crystal sensors 4 cm on a side, or a 4×4 array.

As another modest update relative to *NuSTAR*, the *HEX-P* ASIC will use new readout technology and analog-to-digital converters that were not available when *NuSTAR* was in development. Optimizing the readout scheme will both improve the throughput of the ASIC and reduce the read time by an order of magnitude, from 2.5 ms to ~0.25 ms, This will increase the instrument livetime, allowing measurements of count rates up to ~10,000 cts/s per module when observing bright targets (as compared to the 400 cts/s limit on *NuSTAR*). This will also extend the usable range of the detectors to 200 keV and optimize their gain linearity over that bandpass.

The current approved APRA grant is expected to bring the ASIC to TRL 5.

5. ORGANIZATION, PARTNERSHIPS, AND CURRENT STATUS

Organization of the *HEX-P* mission is based on the highly successful *NuSTAR* mission. As with *NuSTAR*, GSFC will produce the segmented optics. *NuSTAR* multilayer coatings were a Danish contribution by DTU-Space, and a similar arrangement is under discussion for *HEX-P*. Domestic multilayer coating facilities are also available and under consideration (e.g., at GSFC). GSFC will lead assembly of the multi-shells. As with *NuSTAR*, Caltech will lead development and production of the focal plane modules. Discussions between all key instrument partners are mature, though final decisions on instrument and spacecraft participating organizations will await a Probe Announcement of Opportunity.

6. SCHEDULE

HEX-P would be launch-ready in 80 months from the beginning of Phase A. All technology would be matured, and optics production, the critical path, will have started within 18 months of authority to proceed. The development schedule is phased to match the optics production with the spacecraft development starting at month 34 and observatory integration beginning at month 66. Assuming a 2024 start, launch would be in 2031, well matched to the 2031 planned launch of *Athena*. The baseline mission includes a 2-month period after launch for in-orbit check-out (including deployment and calibration), followed by a 60 month operational lifetime consisting, primarily, of a funded GO program with standard ~15% reserves for calibrations, contingency, and serendipitous ToOs. Following in the tradition of previous NASA high-energy missions such as *Chandra*, *Swift*, and *NuSTAR*, *HEX-P* is designed with no consumables and could be expected to continue producing fruitful science for a much longer period, reaching into the 2040s.

7. COST ESTIMATES

We provide a ROM cost based on *NuSTAR* combined with cost models to demonstrate that *HEX-P* is consistent with a Probe-class mission. The *HEX-P* Phases A-F cost estimate is $800M (FY20), which includes the launch vehicle and five years of science operations. All aspects of the mission have a TRL of 5 or higher, or have a path to reach that TRL level over the next 36 months. The cost estimate is provided in Table 5 and is based on the following methodology and assumptions:

Project Management (PM), Systems Engineering (PSE) and Safety and Mission Assurance (SMA): The cost is calculated as 12% (4% PM, 4% PSE, 4% SMA) of the payload, spacecraft, and ATLO cost (excluding reserves). The percentage is based on comparable historical mission averages; *NuSTAR* is 11.3%.

Science: The development portion of the cost (Phases A-D) is calculated as 2% of the payload, spacecraft, and ATLO cost, scaled to *NuSTAR* actuals for the longer development. The operations cost (Phases E-F) is ~$8M per year for data analysis, based on *Spitzer* actual costs.

Payload. The instrument cost is developed using the NICM subsystem model normalized to the *NuSTAR* CADRE values and scaled for mass by payload component. The optics and the other payload components were scaled to the *HEX-P* mass separately as the large amount of inactive mass in the optics otherwise invalidates simple scaling. The estimate was then validated using PRICE-H calibrated to *NuSTAR* to ensure reasonableness.

Spacecraft: The spacecraft cost was developed using the Small Satellite Cost Model (SSCM) normalized to the *NuSTAR* and *ICON* actual costs and then scaled for the partial redundancy and higher mass and power required for *HEX-P*. The estimate was then

WBS	Dev	Ops	Total	Notes
PM/PSE/SMA	47	8	55	Average historical mission wrap rates
Science	8	41	49	Dev based on *NuSTAR*; Ops based on *Spitzer*
Payload	239		239	NICM model scaled to *NuSTAR*; CADRE for optics; parametric mass scaling for remainder
Spacecraft	138		138	SSCM+PRICE model; includes ATLO
MOS/GDS	9	72	81	Dev based on *NuSTAR*; Ops based on *Spitzer* (includes GO program)
Launch Vehicle (LV)	75		75	FY19 costs for an LSP-acquired Falcon 9 inflated to FY20
Pub. Comm.	1	2	3	0.5% of Phase A-F cost (w/o reserves)
Reserves	133	27	158	30% Phase A-D, w/o LV; 15% Phase E-F
Total	**650**	**150**	**800**	

Table 5. *ROM cost estimate ($M, FY20).*

validated using PRICE-H to ensure reasonableness.

Mission Operations Systems/Ground Data Systems: The development portion of the cost (Phases A-D) was calculated as a percentage of the payload, spacecraft, and ATLO cost. The percentage is based on the *NuSTAR* actual costs. As *HEX-P* will be a Guest Observatory, similar in structure to *Spitzer*, the operations cost (Phases E-F) is based on the *Spitzer* actual costs per year.

Launch Vehicle: Although no launch vehicle has been selected, the mass of *HEX-P* is well within the Falcon 9 capability for the *HEX-P* orbit and the cost has been estimated based on recent procurements of that vehicle by Launch Services Program (LSP).

These costs were developed by UC Berkeley as part of the *HEX-P* team, and are early Pre-Phase A estimates that are not a commitment by any institution.

REFERENCES

Aird, J., Coil, A.L. & Georgakakis, A., et al. 2015, MNRAS, 451, 2

Ananna, T.T., Treister, E. & Urry, C.M., et al. 2019, ApJ, 249, 2

Bachetti, M., Harrison, F.A., Walton, D. J., et al. 2014, Nature, 514, 202

Blecha, L., Snyder, G. & Satyapal, S., et al. 2018, MNRAS, 478, 3

Bower, G.C., Chatterjee, S., Cordes, J., et al. 2018, Science with a Next Generation Very Large Array, ASP Conference Series, Vol. 517

Brandt, W.N. & Alexander, D.M. 2015, The Astronomy and Astrophysics Review, 23, 1

Brejnholt, N.F., Soufli, R., Descalle, M.-A., et al. 2014, Opt. Express, 22, 15364

Civano, F., Marchesi, S., Comastri, A., et al. 2016, ApJ, 819, 62

Chen, Z., Gou, L., McClintock, J.E., et al. 2016, ApJ, 825, 45

Del Moro, A., Alexander, D.M., Aird, J.A., et al. 2017, ApJ, 849, 57

Dove, J.B., Wilms, J., Maisack, M., & Begelman, M.C. 1997, ApJ, 487, 759

Fabian, A.C., Lohfink, A., Kara, E., et al. 2015, MNRAS, 451, 4375

Fabian, A.C., Parker, M.L., Wilkins, D.R., et al. 2014, MNRAS, 439, 2307

Fernández-Perea, M., Descalle, M.-A., Soufli, R., et al. 2013, Phys. Rev. Lett., 111, 027404

Fragos, T. & McClintock, J.E. 2015, ApJ, 800, 17

Fürst, F., Walton, D.J., Harrison, F.A., et al. 2016, ApJL, 831, L14

García, J.A., Steiner, J.F., McClintock, J.E., et al. 2015, ApJ, 813, 84

Gilli, R., Comastri, A., Hasinger, G., et al. 2007, A&A, 463, 79

Girou, D.A., Massahi, S., Sleire, E.K., et al. 2015, Development of Ni-based Multilayers for Future Focusing Soft Gamma-ray Telescopes, Vol. 9603

Haardt, F. 1993, ApJ, 413, 680

Harrison, F.A., Craig, W.W., Christensen, F., et al. 2013, ApJ, 770, 103

Harrison, F.A., Aird, J., Civano, F., et al. 2016, ApJ, 831, 185

Hickox, R.C. & Markevitch, M. 2007, ApJ, 661, 2

Hopkins, P.F., Hernquist, L., Cox, T.J., et al. 2006, ApJS, 163, 1

Hornschemeier, A.E., Wolter, A., & Kim, D.-W. 2016, Proceedings of the IAU, Vol. 29B, 124

Joensen, K.D., Hoghoj, P., Christensen, F.E., et al. 1994, Multilayered Supermirror Structures for Hard X-ray Synchrotron and Astrophysics Instrumentation, Vol. 2011

Lansbury, G.B, Alexander, D.M., Del Moro, A., et al. 2014, ApJ, 785, 17

Lansbury, G.B., Gandhi, P., Alexander, D.M., et al. 2015, ApJ, 809, 115

Lanzuisi, G., Gilli, R., Cappi, M. et al. 2019, ApJL, 875, L20

Lazzarini, M., Hornschemeier, A.E., Williams, B.F., et al. 2018. ApJ, 862, 28

Lohfink, A.M., Ogle, P., Tombesi, F., et al. 2015, ApJ, 814, 24

Maccarone, T.J., Yukita, M., Hornschemeier, A., et al. 2016, MNRAS, 458, 3633

Madsen, K.K, Broadway, D., Christensen, F.E., et al. 2018, Proc SPIE, Vol. 10699

Markoff, S., Nowak, M.A., & Wilms, J. 2005, ApJ, 635, 1203

Masini, A., Comastri, A.,Civano, F., et al. 2018, ApJ, 867, 162

Matt, G., Perola, G.C., Piro, L., & Stella, L. 1992, A&A, 257, 63

McClintock, J.E., Narayan, R., & Steiner, J.F. 2014, ApJ, 183, 295

Miralda-Escude, J. & Gould, A. 2000, ApJ, 545, 847

Mori, K., Gotthelf, E.V., Zhang, S., et al. 2013, ApJ, 770, 23

Muno, M., Bauer, F.E., Baganoff, F.E., et al. 2009, 181, 110

Narayan, R. & McClintock, J.E. 2012, MNRAS 419, L69

Psaltis, D., Wex, N., & Kramer, M. 2016, ApJ, 818, 121

Rajwade, K.M, Lorimer, D.R., & Anderson, L.D. 2017, MNRAS, 471, 730

Ramo, S. 1939, Proceedings of the IRE 27, No. 9. IEEE, 584

Shockley, W. 1938, Journal of Applied Physics 9, 635

Steiner, J.F., McClintock, J.E., & Narayan, R. 2013, ApJ 762, 104

Stern, D., Lansbury, G.B., Assef, R.J., et al. 2014, ApJ, 794, 102

Ueda, Y., Akiyama, M., Hasinger, G., et al. 2014, ApJ, 786, 104

Uttley, P., Cackett. E., Fabian, A.C., et al. 2014, ARA&A, 22, 72

Vulic, N., Hornschemeier, A.E., Wik, D.R., et al. 2018, ApJ 864, 150

Wik, D.R., Lehmer, B.D., Hornschemeier, A.E., et al. 2014, ApJ 797, 79

Windt, D.L. 2015, Advancements in Hard X-ray Multilayers for X-ray Astronomy, Vol. 9603.

Windt, D.L., Christensen, F.E., Craig, W.W., et al. 2000, X-ray Multilayer Coatings for Use at Energies Above 100 keV, Vol. 4012.

Windt, D.L., Donguy, S., Hailey, C.J., et al. 2003, W/SiC X-ray Multilayers Optimized for Use above 100 keV, Vol. 4851

Xue, Y.Q., Wang, S.X., Brandt, W.N., et al. 2012, ApJ, 758, 129

Yan, W., Hickox, R.C., Hainline, K.N., et al. 2019, 870, 33

Yao, Y., Chalifoux, B.D., Heilmann, R.K., et al. 2019, Journal of Astronomical Telescopes, Instruments and Systems, 5, 1–9–9

Yukita, M., Hornschemeier, A.E., Lehmer, B.D., et al. 2016, ApJ, 824, 107

Zappacosta, L., Comastri, A., Civano, F., et al. 2018, ApJ, 854, 33

Zdziarski, A.A., Lubinski, P., Gilfanov, M., & Revnivtsev, M. 2003, MNRAS, 342, 355

Zhang, W., Allgood, K.D., Biskach, M., et al. 2019, Journal of Astronomical Telescopes, Instruments and Systems, 5, 1–10–10